MECHANICAL AND THERMAL BEHAVIOR FOR MACHINING TI-6AL-4V WITH $AlMgB_{14}$ AND WC-Co TOOLS

L. Deshayes[1]
IFMA-Lami, Clermont Ferrand, France
Email : ldeshaye@cme.nist.gov

J. L. Evans
Engineering Institute, Farmington, AR 72730
jeffevans@renfroe.com

R. Ivester[2]
NIST Manufacturing Engineering Laboratory
Gaithersburg, Maryland USA
Email : robert.ivester@nist.gov

D. G. Bhat
Department of Mechanical Engineering,
University of Arkansas, Fayetteville, AR 72701
dgbhat@engr.uark.edu

S. A. Batzer
Renfroe Engineering, Farmington, AR
batzer@renfroe.com

ABSTRACT

Many of the currently used tool materials will dissolve, diffuse, and/or react with titanium due to high temperatures at the tool/work-piece interface. Potential next generation tool materials that would improve the machining of titanium and eliminate the contamination of the work-piece are being developed. One such material, $AlMgB_{14}$, is the subject of the research presented in this paper.

Specimens of the newly developed tool, $AlMgB_{14}$ were fabricated into a standard tool geometry. This tool material was compared with a standard WC-Co tool material to machine a Ti-6Al-4V work material. Thermal and force measurements were conducted using both types of tools during orthogonal cutting. Results are also compared with finite element simulations. The paper outlines that higher temperatures are obtained by $AlMgB_{14}$. It is also shown that this material is more appropriate to be used with high cutting speeds. Nevertheless, a weakness of this newly developed $AlMgB_{14}$ is its toughness that needs to be improved for better performance in an industrial environment.

[1] Laurent Deshayes is currently a guest researcher at the National Institute of Standards and Technology.
[2] Official contribution of the National Institute of Standards and Technology; not subject to copyright in the United States.

1 INTRODUCTION

Titanium alloys are finding increasing use in a variety of applications. These materials have excellent corrosion resistance, fatigue strength, fracture resistance, and strength-to-weight ratio that make them attractive to the automotive, biomedical, petroleum, and chemical industries [1]. Given this very desirable combination of properties, the primary application of these alloys has been in critical turbine engine components and airframes for the aerospace industry [2]. The primary obstacle to more widespread use of titanium is that it is expensive to extract, process, fabricate, and machine [2, 3].

Titanium and titanium alloys are classified as difficult-to-machine materials for a variety of reasons. They have a low thermal conductivity, high chemical reactivity at temperatures above 500°C, low modulus of elasticity, and high strength at elevated temperature. The low thermal conductivity combined with small chip thickness, generally used in machining titanium, causes a small contact area and subsequently high stresses and temperatures at the tip of the tool. The high temperatures increase the reactivity of the titanium work piece with the tool materials. Deflection and chatter are problems associated with a material having a low modulus of elasticity. Even at the elevated temperatures caused during machining, titanium retains its strength, and this suppresses the plastic deformation needed to form a chip [4].

The high stresses and high temperatures present at the tool/work-piece interface can cause significant surface damage to the titanium alloys [5]. Contamination and damage of the titanium work-piece via diffusion of tool material and atmospheric constituents can lead to degradation of mechanical properties, especially the fatigue strength [6, 7].

Over the last few decades, significant advancements have been made in the development of cutting tool materials, which have greatly increased the machining productivity of steels, cast

irons, nickel-based alloys, and many other metallic materials. However, due to the previously mentioned unusual characteristics of titanium, satisfactory improvements have not yet been made in the cutting of its alloys [8-10]. It is necessary to machine titanium with high speeds and a large chip cross-section in order to achieve high productivity and reduce machining costs.

Highly alloyed high speed steels, such as M42, M40, and M33, have had some success in machining titanium alloys at low speeds [1], but they have also been known to cause significant surface damage to the titanium work-piece and exhibit catastrophic failure during machining. Cubic boron nitride, polycrystalline diamond, and natural diamond have had some promising results when machining titanium, but their high cost of approximately $(US) 15,500 per kilogram [11] has limited their use [2, 9]. The Al_2O_3 based ceramics and SiAlON materials were found to be unsuitable for this application [2, 8, 9]. Uncoated WC-Co materials have proven to be the appropriate tools for machining titanium, but even with these tools the cutting speeds for machining creep resistant titanium alloys must be kept low, such as 30 m/min [12]. Conventional machining of titanium alloys is in the range of 30 m/min to 100 m/min [1]. Higher wear rates were seen with coatings such as TiN, TiC, TiB_2, HfN, Al_2O_3, and multilayer coatings of these materials, than with straight grade WC-Co [2, 5 , 8, 9, 13-15]. Some results show that a boron carbide coated WC-Co material has a limited tendency to diffusion bond to titanium and may be a suitable material for machining titanium [16]. Ion implantation of the WC-Co tool has shown some promising results [17, 18, 19], as has a PVD coating of MoS_2 solid lubricant [19].

Several types of wear patterns during machining of titanium alloys occur, such as attrition, adhesion, and, one of the most pervasive for WC-Co and CBN tools, dissolution-diffusion [1, 8, 9, 13, 20]. Attrition and adhesion seem to control the growth of the wearland on the flank face. Dissolution-diffusion wear is the primary factor contributing to crater growth on the rake face of

the insert. Temperatures at the tool tip while machining titanium have been measured to be between 900 and 1100 °C for some tool materials [1, 21]. Thermal conductivity is very low for titanium (7 W/m K for Ti-6Al-4V compared to 50 W/m K for low carbon steel) and this does not allow for much heat dissipation through the work-piece [22]. Approximately 80 % of the total heat generated during machining is conducted through the tool [9], causing strength reduction in the tool and increased diffusion rates at the rake face and flank. The tool and work-piece interface is in intimate contact and leads to diffusion bonding and dissolution of the tool material into the chip and work-piece. If a reaction boundary layer, such as TiC, forms between the work-piece and tool material, then the diffusion flux can be minimized and the diffusion-dissolution wear mechanism is retarded [23].

2 CUTTING TOOL MATERIALS

To adress these issues, the first option is to use a tool material that does not cause the contamination or damage that is presently a problem with machining titanium and its alloys. This would eliminate the chemical milling step, thereby reducing the cost of this material. The ideal tool material will have very high hardness, high temperature stability, low solubility with titanium, lower thermal conductivity than titanium, and good fracture toughness [14]. Some theoretical investigations have been conducted on the use of rare earth compounds as tool materials for machining titanium alloys [14]. There have also been some increased developments in the area of boride based tool materials that would be suitable for this application. Some of these compounds exhibit a very high hardness, high temperature stability, and low solubility into titanium [14, 25, 26].

For the tests presented in this paper two uncoated tool materials have been selected for all experiments. The first one is a tungsten carbide with 6 % cobalt and the second one a recently

developed ultra-hard aluminum-magnesium-boron composite ($AlMgB_{14}$). The first tool material has been chosen as a "common" used material for machining titanium in order to make suitable comparison with the newly developed $AlMgB_{14}$ tool material. $AlMgB_{14}$ was selected in this study for its good properties to machine titanium such as presented in previous studies [34] .

Researchers at Ames National Laboratory in Ames, Iowa have shown that $AlMgB_{14}$ has exceptionally high hardness (32-35 GPa), and that the hardness can be increased (to at least 45-50 GPa) by additions of certain elements and compounds [27]. These modified boride compounds rank alongside cubic boron nitride as the second hardest material known [28, 29], as is shown in Table 1. The structure of the complex ternary intermetallic $AlMgB_{14}$ is shown in Fig. 1. The most recently developed compositions of this boron-based hard material are receiving significant interest due to their attractive properties. Some of the more fundamental material properties are being evaluated such as coefficient of thermal expansion, electronic structure, and elastic properties [30]. Preliminary studies have been conducted using $AlMgB_{14}$ as a cutting tool. This material, in the form of a disk (not a standard cutting tool geometry) has shown very promising results in the machining of 6061 aluminum, 304 stainless steel, Inconel, and concrete at various cutting rates [31]. This ultra-hard boride material has also been laser deposited as a coating on carbide inserts for lathe turning of titanium [32]. Those coated tools out-performed uncoated carbide and performed about as well as the commercially available TiAlN coated inserts.

Previous work on $AlMgB_{14}$ by Bedekar [33-35] at the University of Arkansas showed promising chemical compatibility of this material with titanium. Thermodynamic-based total solubility calculations were performed which indicated significant resistance to chemical wear in the machining of titanium. Bedekar [35] also conducted diffusion studies and showed that

$AlMgB_{14}$ reacted to a lesser degree with titanium alloys than did cemented carbide cutting tools. The diffusion experiments were conducted by coupling the tool material and titanium work-piece together in vacuum at 1000 °C for 120 hours. The couples were then sectioned and analyzed using Electron Probe Micro Analysis. The primary interaction mechanism for $AlMgB_{14}$ was the diffusion of boron along the Ti-6Al-4V grain boundaries. The diffusion zone present in the Ti-6Al-4V when coupled with $AlMgB_{14}$ was 40 μm, and the diffusion zone observed when Ti-6Al-4V was in contact with WC-Co was 250 μm. These results gave evidence that $AlMgB_{14}$ has the potential of being a successful cutting tool material for machining Ti-6Al-4V in terms of its chemical stability. The results of Bedekar led to this present work, which is aimed at evaluating the performance of a bulk $AlMgB_{14}$ cutting tool insert with the TPG-222 tool geometry in the lathe turning of Ti-6Al-4V.

Concerning the process to obtain $AlMgB_{14}$ inserts for this research, Ames Laboratory, processed the $AlMgB_{14}$ material via a powder metallurgy technique. The process consisted of weighing the aluminum, magnesium, and sub-micron boron elemental constituents in a helium filled glove box. Next the mixture was transferred to a hardened steel Spex mill and mechanically alloyed for 12 hours with hardened steel media. The resultant loose powder was transferred to a boron nitride-lined graphite die. This die assembly was transported to a controlled atmosphere hot press, positioned, and evacuated. The chamber was back-filled with argon establishing a slight positive pressure. While the furnace was being ramped at 10 °C /min to 1400 °C, a compressive stress of approximately 13 MPa was gradually applied to the die assembly. The applied compression was increased to 104 MPa for the duration of the 60 minute hold at 1400 °C. The pressure is then released and the furnace allowed to cool to ambient

temperature at a rate of 20 °C/min. Finally, the compact is ejected from the die by application of a uni-directional load from a cold press.

3 EXPERIMENTAL SET UP

3.1 Work-material

A bi-phase Ti6Al4V alloy has been considered for the experiments. Its microstructure, given in Fig. 2 shows small stabilized β phases; α phases are much bigger grains. For the experiments, a tube work-piece was used to conduct orthogonal cutting experiments. Its dimensions were approximately an output diameter of 88.64 mm and an inner diameter of 84.91 mm. Thereby the tube thickness was approximately 1.87 mm. The tube was machined from solid round stock leaving enough material at one end to bolt the workpiece to the faceplate of the lathe such as shown in previous publications [36]. Preparation of the cylindrical surface of the tube included precision turning of the surface to a sub-micrometer level of surface roughness and cylindrical form error of less than 5 micrometers in order to control both the thickness of the tube as well as the quality of the surface to be imaged (see section 3.3 for more details).

A second work-piece has been used to conduct initial test in single point turning. Its initial dimension was a bar of 90 mm in diameter and 270 mm length.

3.2 Cutting tool preparation

A triangular tool geometry, TPG-222 (defined in ISO 1832 [37]), with a flat cutting face was chosen for this process, since this was the first time this $AlMgB_{14}$ based material was to be fabricated into a standard cutting tool geometry, but also because of its extreme hardness. In addition this geometry was chosen in order to compare this $AlMgB_{14}$ based material to tungsten carbide-based insert's generally used for machining titanium, with a commonly available

geometry (a TPG-222, grade K313 from Kennametal[3]). For both tools and all experiments, a normal cutting angle of 0° was used.

Figure 3 shows this insert geometry whose dimensions are given in Table 2. The cutting edge was sharp with a radius less than 5 microns. In the case of orthogonal cutting, a tool holder made of high speed steel was prepared in order to present the cutting edge perpendicularly to the tube wall. For single point turning a cutting edge angle of 90° was selected for the tool holder. The insert was top clamped.

In order to qualify the tool materials hardness and brittleness, testing was done using Vickers micro-hardness tests with a load of 1kg. This showed a 1800 HV1 hardness for the WC/Co cutting tool and 2240 HV1 for the AlMg B_{14} tool. Results are more detailed in [38].

3.3 Force and Thermal Measurements

Force and thermal experiments were conducted using the $AlMgB_{14}$ and WC-Co tool inserts. Orthogonal cutting tests were carried out on the NIST[1] precision machining testbed consisting of a diamond turning class Ex-Cello air-bearing spindle mounted on a Moore-3 base. The testbed includes a custom tool post incorporating a Kistler[1] 9257b dynamometer at the base, and a removable insert holder to facilitate tooling changes. The experimental configuration approximates orthogonal cutting by plunging a tool into the wall of the cylindrical tube (presented in sub-section 3.1) and across the entire wall thickness as in prior experiments at NIST [36] and elsewhere. The force data were collected using the Kistler Dynamometer through a Nicolet Odyssey XE[1] Oscilloscope at a sampling rate of 500 KHz.

[3] Commercial equipment and materials are identified in order to adequately specify certain procedures. In no case does such identification imply recommendation or endorsement by the National Institute of Standards and Technology, nor does it imply that the materials or equipment are necessarily the best available for the purpose. Official contribution of the National Institute of Standards and Technology; not subject to copyright in the United States.

Thermal measurements of machining were obtained from a combination of a high-speed infrared video camera with an infrared/visual beam splitter and a high-speed visual spectrum video camera, as shown in Fig. 4. The thermal data were collected at a rate of 300 Hz and the visual information at a rate of 6 kHz. The visual/infrared beam splitter enables simultaneous imaging using two synchronized cameras with the perspective shown in Fig. 5. The visual spectrum video enables direct observation of surface condition, chip morphology, and chip flow, and incorporates a lighting system using a beam splitter and a fiber optic light source. Visual spectrum images enable aberrations to be distinguished from inherent process variability. For example, the visual camera indicated when the curling chip obscured the view of the thermal camera causing the temperature data to be skewed one way or the other [39]. Additionally, deviations from the focal plane result in loss of focus readily observable in visual spectrum images, as opposed to infrared images where image content lacks adequate detail to assess focus.

Proper orientation of the visual/infrared beam splitter approximately centered the infrared field-of-view within the larger visible field of view. Adjustment of the relative positioning of the optical components approximately centered the visible depth of field within the larger infrared depth of field. In this way, a target focused and centered in the visible camera is in focus at the same time in the infrared camera. A historical review about measurement quality is given in [39].

The integration time of each camera serves a similar role to an analog camera's shutter speed. Increasing the integration time improves the camera's sensitivity to gradients until the signal levels reach the saturation limit. Decreasing the integration time reduces blurring of the image due to motion of the subject. The integration times were 167 μs for the visible camera and 192 μs for the infrared camera.

4 EXPERIMENTAL RESULTS

4.1 Single point turning observations

Single-point turning experiments were conducted on a CNC Lathe. All test conditions are given in Table 3. The first test conducted was with the WC-Co insert J-1. This test was conducted using a surface speed of 75 m/min, a depth of cut (DOC) of 1.5 mm, and a feed of 0.25 mm/rev. These cutting parameters are the ones commonly used in industrial applications for such tool material. This test successfully cut the Ti-6Al-4V material. However, during the machining, a red glow, near the tool-chip interface was observed. The tool insert was examined with an optical microscope. Photographs of the insert, before testing and after testing, are seen in Fig. 6a. A crater wear pattern is apparent on the rake face of the insert and indicates, as expected, a normal wear behavior of this material.

The next test performed was using the $AlMgB_{14}$ cutting tool insert, A-1, with the same cutting conditions as was used with J-1 to evaluate the new boride-based material. At the contact with the part to be cut the tool catastrophically failed fracturing into several pieces. The before and after photos of this insert are shown in Fig. 6b. The result of this first test required a reduction in speed and depth of cut in order to more adequately assess the capabilities of this new material. Under less severe machining conditions, with insert B-2, the end of the nose of the tool chipped off during this test. Insert B-2 with the chipped nose can be seen in Fig. 6c.

$AlMgB_{14}$ inserts U-1 and R-1 were tested at 45 m/min and 30 m/min, respectively. These two inserts appeared to perform well at these cutting conditions. Three successive tests were conducted with each of the inserts (the number 3 in parentheses in Table 3 denotes the three tests which were conducted). The nose was inspected in between each test. The WC-Co inserts L-1 and K-1 were used to machine the Ti-6Al-4V bar using the same cutting conditions as U-1 and

R-1. This allowed the two materials to be compared. Both materials appeared to give similar results. At the end of the third test with R-1 a small chip was removed from the nose, causing the nose to have a slightly irregular shape. Inserts U-1, K-1, and L-1 all had similar appearances. Each of them had a small wear notch on the rake face after the third test. The notch on the WC-Co inserts appeared to be shallower than the notch present on the $AlMgB_{14}$ insert. Since some built up edge was observed on the cutting tool made of $AlMgB_{14}$, it indicates that this tool-material ($AlMgB_{14}$) – work-material (Ti-6Al-4V) interaction perform better at higher cutting speeds.

Ames Lab provided two other batchs of $AlMgB_{14}$. Experiments showed that these materials were as weak as the previous inserts. Thereby additional tests were performed at higher cutting speeds using inserts obtained from the first batch of material. In order to keep the inserts from catastrophically failing immediately, the DOC had to be reduced significantly to reduce the applied stresses on the tool insert. Insert G-1, used with a cutting speed of 120 m/min and feed of 0.05 mm/rev, appeared to perform the best during this set of tests. No visible chips adhered to the surface of this tool. The WC-Co insert labeled P-2 had a small fragment of the work-piece stuck to the rake face after machining.

From these preliminary tests, it is concluded that the $AlMgB_{14}$ tool insert fracture toughness is inferior to the inserts made of WC-Co material. Due to this lack of sufficient mechanical integrity, tool wear measurements and tool life calculations could not be performed. Therefore, before producing new material batch or insert geometries to reduce such problems, more advance experiments were performed to focus on the material behavior for machining titanium using orthogonal cutting conditions. These are discussed next.

4.2 Orthogonal cutting measurements

Cutting forces and radiance temperatures were measured using the set up presented in section 3.3. Because of the preliminary single point turning tests results, the effect of cutting speed was studied with a feed rate fixed at 0.05 mm/rev for all experiments. This feed value was also convenient on one hand to obtain a thermal image in the field of view of the camera and on the other hand to be able to perform the tests on the Moore lathe whose feed values have to be less than 0.1 mm/rev. The tube thickness was about 1.87 mm; 3 levels of cutting speed, 60, 120, and 180 m/min, were used for the experiments plan. Table 4 summarizes the results, where *WC* indicates the results for the WC-CO inserts, and *Al.* for the ceramic inserts.

Measured specific cutting cutting forces, $Kcx_{measured}$ (corresponding to the cutting force $Fx_{measured}$, in the cutting speed direction) and $Kcy_{measured}$ (for Thrust force $Fy_{measured}$, perpendicular to the cutting speed value, here in the feed direction) are generally higher for the ceramic tool, except for the higher cutting speed value. Based on other published results [40] it may indicate a limit in the tool resistance. Thereby one may conclude that ceramic tools present better performances at higher speeds.

Concerning radiance temperatures, the radiance is bigger for chips obtained with the ceramic tool for all cutting speeds. If one assumes that the emissivities of the chips are all comparable (see section 5), then this indicates that more heat was transferred to the chip by using the ceramic tool. It confirms the observation made based on cutting forces analysis.

4.3 Chip characteristics

Figure 7 shows the typical chip morphology for chips produced with the $AlMgB_{14}$ inserts, on the right, and those produced with the WC-Co inserts, on the left. The chip generated from machining with $AlMgB_{14}$ has a much smaller curl than the one obtained with the WC-CO tool.

The chip is much tighter, correlating the previous experimental results, that the temperature of the chip was higher causing the chip to soften and deform more readily during the machining process.

Chips obtained for each cutting speed and cutting tool were mounted, polished and etched with a solution of 95 ml distilled water, 3 ml nitric acid (HNO_3), and 2 ml hydrofluoric (HF). This etchant (also called Kroll etchant) was wiped on the sample for 1 min before being cleaned with distilled water. Results are similar to the one shown in Fig. 8 and show very similar chip morphology for both cutting tool materials. From the pictures we can observe that chip widths obtained with the ceramic insert are higher than those obtained with the carbide insert. This indicates that thermal softening is higher with the ceramic insert.

Measured chips dimensions, for each cutting speed, are given in Table 4. The average chip width, e, shows that for small cutting speeds, the WC-Co tool presents a slightly bigger value, while for higher cutting speeds the ceramic tool provides larger chips. The e_{min} (see Fig. 8) value is a minimum averaged value of the bottom teeth. The e_{max} value is the average value of the top teeth. Measurements confirm that with the ceramic insert chip segmentation and localized shear band occurs with smaller cutting speeds than using the carbide insert. Also, the difference between e_{min} and e_{max} is much higher for the ceramic tools, which confirms that more heat is transferred to the chip facilitating thermal softening, damage and consequently instable mechanical oscillations. Such behavior is typical for titanium alloys and high speed machining [41].

4.4 SEM Analysis of the $AlMgB_{14}$ Cutting Tool Inserts

A preliminary failure analysis investigation was conducted to determine why the $AlMgB_{14}$ inserts fractured so readily during the machining tests. The $AlMgB_{14}$ ceramic material has a very

high hardness and very limited resistance to crack propagation as was seen during the machining tests and is described in more detail in [42]. This lack of fracture resistance is a result of the brittle nature of ceramics. Brittle solids are flaw-limited meaning cracks are more likely to grow quickly and cause catastrophic failure under low stress if flaws of some variety are present. The SEM revealed a rather large amount of microporosity, which apparently formed during processing. The disks of $AlMgB_{14}$ required for fabrication of these tools were thicker than those previously produced at Ames Lab and they did not have the capabilities to provide sufficient compaction pressure to fully densify the material. This lack of adequate compaction pressure of the metal powders is the most likely reason for the porosity. The micro-porosity that led to the failure of the inserts can be seen in fig. 10b.

Another microstructural factor also apparently contributed to the failure of the $AlMgB_{14}$ inserts. This boride-based material is multi-phased. One constituent has a long blocky appearance. The crack appears to have found its path of least resistance at the interface of this long acicular component and the rest of the bulk material. The interfacial bond may have insufficient strength allowing the crack to easily propagate through it. Figure 10c shows the crack along this interface.

5 FEM SIMULATIONS RESULTS

FEM simultations have been run in order to compare simulated temperatures and cutting forces with experimental results. The constitutive model used for simulations is a strain-rate and temperature dependent visco-plastic material model such as documented in [43]. More details about material behavior are given in [44] and are not discussed in this work. Calculations are performed using the Thirdwave Systems' Advantedge code package dedicated to metal cutting

[45]. This package uses a Lagrangian finite element model based on adaptive meshing to correct problems due to element distortion. The present FE study concerns a two-dimensional representation of cutting conditions.

A cutting tool with a mean normal rake angle of 0° with a flat cutting face has been used. For the AlMgB14 tool material, the Thirdwave System's Advantedge predefined material named "Cermic-general" material has been used, and the material named "Carbide-General" for the WC-CO tool. The work material used in the simulation was a Ti6Al4V whose chemical compositions were close to the material used for our experiments and described in section 3.1. Finally, simulations were run under orthogonal cutting conditions. In order to simulate more precisely the serrated chips observed in the experiments due to thermo-mechanical oscillations induced in metal cutting on one hand, and to minimize time simulation on an other hand, a minimum element size of 0.02 mm has been chosen. In Fig. 11, it is observed that the oscillation of cutting force, due to shear band formation, is well simulated. In addition, it is observed that plastic strain and cutting forces are accurately determined for such a minimum mesh size.

Table 7 provides the results obtained with simulations. The comparison with experimental results provided in Table 4 confirm the previous conclusion about temperatures and cutting forces. Nevertheless, notice that during the experiments radiance temperatures were measured while simulations provide true temperature (in °C). Based on FE results for true temperature and experiments for radiance temperatures, the emissivity, e, is calculated [39] by:

$$e=\exp\left(\frac{1438.10^{2}*\left(1-\frac{T_{true}+273}{T_{rad}+273}\right)}{\left(T_{true}+273\right)*3250}\right),$$

Where T_{true} is the True temperature and T_{rad} the radiance temperature. Using Ttrue and Trad from Tables 7 ansd Table 4 respectively, the chip emissivity is 0.69 ± 0.02 for the chip produced with

WC-Co inserts and 0.78 $\pm$ 0.025 for the $AlMgB_{14}$ insert. Finally, to check the emissivity value, additional experimental studies such as given in [39] are required.

6 CONCLUSION

This work was motivated to compare the machining of titanium alloys of a newly developed ceramic tool material, $AlMgB_{14}$, with a more "conventional" tungsten carbide, WC-Co, tool material generally used in industry to cut such work material. Experimental results, confirmed by finite element simulations, clearly showed that the ceramic tool material presents the good property of transferring more heat into the chip. In addition cutting forces are decreasing at higher cutting speeds. This two observations let us believe that this material performs better at higher cutting speeds compared to the WC-Co tools.

Improvement on processing this $AlMgB_{14}$ material, to obtain better failure toughness, are necessary in order to obtain high performances in machining titatium and make it interesting for industrial applications. Due to a better transfer of heat into the chip, this material may reach better cutting speeds and improve production times.

REFERENCES

[1] Zareena, A.R, Rahman, M.,Wong, Y.S., "High Speed Machining of Aerospace Alloy Ti-6Al-4V," *International SAMPE Technical Conference*, Vol. 33, 739-750, 2001

[2] Machado, A.R., Wallbank, J." Machining of Titanium and its Alloys: A Review," *Proceedings of the Institution of Mechanical Engineers, Part B: Management and Engineering Manufacture*, Vol. 204, n 1, 53-60, 1990.

[3] Kahles, J.F., Field, M., Eylon, D., and Froes, F.H., "Machining of Titanium Alloys," *Journal of Metals*, 27-35, April, 1985.

[4] Yang, X., Liu, R.C., "Machining Titanium and its Alloys," *Machining Science and Technology*, Vol. 3, n 1, 107-139, 1999.

[5] Cotton, J.D., Clark, L.P., Phelps, H.R., "Titanium Alloys on the F-22 Fighter Airframe," Advanced Materials and Processes, Vol 160, n 5, 25-28, 2002.

[6] Williams, D.N., and Wood, R.A., *Effects of Surface Condition on the Mechanical Properties of Titanium and Its Alloys*, Metals and Ceramics Information Center Report, Battelle Columbus Laboratories, 1971.

[7] Boyer, H.E., and Gall, T.L., *Metals Handbook: Desk Edition*, 9th edition, American Society of Metals, Metals Park, Ohio, 1985.

[8] Dearnley, P. A., Grearson, A. N., "Evaluation of Principal Wear Mechanisms of Cemented Carbides and Ceramics Used for Machining Titanium Alloy IMI 318" *Materials Science and Technology*, Vol 2, n 1, 47-58, 1986.

[9] Ezugwu, E.O.,Wang, Z.M., "Titanium Alloys and Their Machinability - A Review," *Journal of Materials Processing Technology*, Vol. 68, n 3, 262-274, 1997.

[10] Ezugwu, E.O.,Wang, Z.M., Machado, A.R., "Wear of Coated Carbide Tools When Machining Nickel (Inconel 718) and

Titanium Base (Ti-6A1-4V) Alloys," *Tribology Transactions*, Vol. 43, n 2, 263-268, 2000.

[11] Ames National Laboratory, Ames Iowa, "Ames Laboratory News Release," October 25, 1999.

[12] Upadyaya, G.S., Cemented Tungsten Carbides: Production, Properties, and Testing, Noyes Publication, Westwood, NJ, 1998.

[13] Brookes, C.A., James, R.D., Nabhani, F., "Aspects of Utra-hard Cutting Tool Wear in the Machining of Titanium Based Aerospace Alloys," *Titanium & Aluminum: Proceedings of the International Conference*, 183-194, 1990.

[14] Kramer, B.M., Viens, D., and Chin, S. "Theoretical Consideration of Rare Earth Metal Compounds as Tool Materials for Titanium Machining," *CIRP Annals*, Vol. 42, n 1, 111-114, 1993.

[15] Che-Haron, C.H., "Tool Life and Surface Integrity in Turning Titanium Alloy," *Journal of Materials Processing Technology*, Vol. 118, n 1-3, 231-237, 2001.

[16] Klaphaak, D.J., "Coated Tools for Machining Aerospace Materials," *Carbide and Tool Journal*, Vol. 19, n 5, 14-16, 1987.

[17] Treglio, J.R., Tian, A., Perry, A.J., "Extending Carbide Tool Lifetime by Metal Ion Implantation," *Surface and Coatings Technology*, Vol 62, 438-442, 1993.

[18] Walter, J.L., Skelly, D.W., and Minnear, W.P., "Ion Implantation of Cobalt-Tungsten Carbide Tools for Machining Titanium," *Wear*, Vol. 170, n 1, 79-92, 1993.

[19] Rechberger, J., Brunner, P., Dubach, R., "High Performance Cutting Tools With a Solid Lubricant Physically Vapour-Deposited Coating," *Surface and Coatings Technology*, Vol. 62, 393-398, 1993.

[20] Min, W., Youzhen, Z., "Diffusion Wear in Milling Titanium Alloys," *Materials Science and Technology*, Vol. 4, n 6, 548-553, 1988.

[21] Bhaumik, S.K., Divakar, C., Singh, A.K., "Machining Ti-6Al-4V Alloy with a wBN-cBN Composite Tool," *Materials & Design*, Vol.16, n 4, 221-226, 1995.

[22] Aronson, R., "What's Different About Manufacturing for Aerospace?" *Manufacturing Engineering*, 50-62, 2002.

[23] Hartung, P.D., Kramer, B.M., "Tool Wear in Titanium Machining," *Annals of the CIRP*, Vol 31, n 1, 75-80, 1982.

[24] Moffatt, W.G., *The Handbook of Binary Phase Diagrams*, Genium Publishing Company, Schenectady, NY, 1984.

[25] Mehrotra, P.K., Ahuja, D.P., and Brooks, H.S., "Group IVB Boride Based Articles, Articles, Cutting Tools, Methods of Making, and Method of Machining Group IVB Based Materials," United States Patent No. 5,632,941.

[26] Cook, B.A., Harringa, J.L.,Lewis, T.L., Russell, A.M., "A New Class of Ultra-hard Materials Based on $AlMgB_{14}$, *Scripta Materialia*, Vol 42, 597-602, 2000.

[27] Cook, B.A., Harringa, J.L., Russell, A.M., Superabrasive Boride and a Method of Preparing the Same By Mechanical Alloying and Hot Pressing," United States Patent No. 6,099,605.

[28] Holleck, H., "Marterial Selection for Hard Coatings," *Journal of Vacuum Science Technology*, Vol. A4, 2661, 1986.

[29] Krar, S.F. and Ratterman, E., *Superabrasives*, McGraw-Hill Publishing, New York, NY, 12, 1990.

[30] Russell, A.M., Cook, B.A., Harringa, J.L., Lewis, T.L., "Coefficient of Thermal Expansion of $AlMgB_{14}$," *Scripta Materialia*, Vol 46, 629-633, 2002.

[31] Cook, B.A., Harringa, J.L., Russell, A.M., Batzer, S.A., "A Proof-of-Concept Study of the Use of Complex Borides for Disassembly of Decommissioned Nuclear Reactor Containment Vessels," *Machining Science and Technology*, Vol 7, n 1, 157-165, 2003.

[32] Cherukuri, R. and Molian, P., "Lathe Turning of Titanium Using Pulsed Laser Deposited, Ultra-Hard Boride Coatings of Carbide Inserts," Machining Science and Technology, Vol 7, n 1, 119-135, 2003.

[33] Bedekar, V., *An Analytical and Experimental Study of Abrasive and Chemical Wear Mechanisms of $AlMgB_{14}$ in Machining of Titanium Alloys*, M.S. Thesis, Mechanical Engineering, University of Arkansas, 2003.

[34] Bedekar, V., Bhat, D.G., Batzer, S.A., Walker, L., and Allard, L., "Chemical Interdiffusion Study of Ultra-hard Ceramic $AlMgB_{14}$ in the Machining of Titanium Alloys," Presented at GSTC Conference, Houston, TX, 2003.

[35] Bedekar, V., Bhat, D.G., and Batzer, S.A., "A Preliminary Study of Chemical Solubility of Ultra-Hard Ceramic $AlMgB_{14}$ in Titanium – Reconciliation of Model with Experiment," Machining Science and Technol., v8(3), 2004, pp. 341-355.

[36] Davies, M.A., Cao, Q., Cooke, A.L., Ivester, R., "On The Measurement And Prediction Of Temperature Fields In Machining 1045 Steel", *CIRP Annals – Manufacturing Technology*, v52, n1, 2003, p.77-80.

[37] ISO 1832, Indexable Inserts for cutting tools – Designation, ISO, 1832 Geneva, 1991, 18 p.

[38] J.L. Evans, L. Deshayes, D.G. Bhat, S.A. Batzer, A Failure Analysis of an Experimental AlMgB14 Cutting Tool, short communication to appear *in proceeding of Microscopy and Micronalysis 2005*, Honolulu, Hawaii, USA, Jully 31st – August 4th 2005.

[39] R. Ivester, E. Whitenton, L. Deshayes, Comparison of Measurements and Simulations for Machining Aluminium. *Transactions of the NAMRC 33* (North American Manufacturing Research Conference) N.Y. May 24-27, Edited by the Society of Manufacturing Engineers, 2005.

[40] Deshayes, L., 2003, Cutting Methodology Study, Link between Couple Workpiece Tool and Machine Tool Workpiece System (Méthodologie d'étude de la coupe, liaison entre Couple Outil Matière et Pièce Outil Machine). Ph.D. Thesis, Insa de Lyon, 271 p

[41] Davies M. A., Burns T. Thermomechanical oscillations in material flow during high-speed machining. *Phil. Trans. R. Soc. Lond. A*, 2001, 359, 821-846.

[42] Evans, J.L., An Evaluation of AlMgB14 as a Tool Material for the Machining of Ti-6Al-4V, M.S. Thesis, University of Arkansas, 2004.

[43] Marusich T.D., Ortiz, M. Modelling and simulation of high-speed machining. *International Journal for Numerical Methods in Engineering*, 38(21), 1995, 3675-3694.

[44] Mabrouki T, Deshayes L, Ivester R, Rigal J.-F, Jurrens K. Material Modeling and Experimental Study of Serrated Chip Morphology. In: Proceedings of the 7th CIRP workshop, Clunny, France, 2004, 53-66.

[45] Thirdwave System's AdvantEdge, www.thirdwavesys.com (December 15th 2004).

LIST OF TABLES AND TABLES

Table 3: Insert materials hardness

Material	**Formula**	**Hardness (GPa)**
Diamond	C	80
Modified Boride	$AlMgB_{14}$ + Alloys	46
Cubic Boron Nitride	BN	45
Baseline Boride	$AlMgB_{14}$	35
Titanium Diboride	TiB_2	30
Titanium Carbide	TiC	28
Silicon Carbide	SiC	26
Titanium Nitride	TiN	21
Tungsten Carbide	WC	24

Table 4: TPG insert's geometry dimension

A (mm)	I (mm)	R (mm)	M (mm)	T (mm)
6.35	11	0.80	8.73	3.18

Table 3: List of machining tests with their cutting parameters

Insert ID	**Tool material**	**Cutting Speed (m/min)**	**Feed (mm/rev)**	**DOC (mm)**
J-1	WC-Co	75	0.25	1.50
A-1	$AlMgB_{14}$	75	0.25	1.50
U-1 (3)	$AlMgB_{14}$	45	0.25	0.25
L-1 (3)	WC-Co	45	0.25	0.25
B-2	$AlMgB_{14}$	30	0.25	0.25
R-1 (3)	$AlMgB_{14}$	30	0.25	0.25
K-1 (3)	WC-Co	30	0.25	0.25
G-1	$AlMgB_{14}$	120.1	0.2438	0.05
P-2	WC-Co	120.0	0.2438	0.05

Table 4: Experimental results for orthogonal cutting tests

Vc (m/min)	**60**		**120**		**180**	
Tool	WC.	Al.	WC.	Al.	WC.	Al.
Radiance temperature	280	360	330	470	360	530
$Fx_{measured}$ (N)	208	216	202	225	223	219
$Fy_{measured}$ (N)	102	143	95	139	122	112
$Kcx_{measured}$ (Mpa)	2015	2095	1959	2178	2161	2121
$Kcy_{measured}$ (Mpa)	985	1390	917	1349	1179	1085

Table 5: Averaged chips dimensions obtained in orthogonal tests

Vc (m/min)	**60**		**120**		**180**	
Tool	WC.	Al.	WC.	Al.	WC.	Al.
e (μm)	59.7	57.9	60.5	60.9	62.5	67.4
e_{min} (μm)	53	53.4	50	47	41	57
e_{max} (μm)	64.4	67	73	77	58	78

Table 6: Simulation results

Vc (m/min)	**60**		**120**		**180**	
Tool	Tool	WC.	Al.	WC.	Al.	WC.
T(°C)	790	850	860	930	980	1060
Fx_{simul} (N)	105	111	110	105	110	104
Fy_{simul} (N)	56	69	70	65	62	60
Kcx_{simul} (Mpa)	2100	2220	2200	2100	2200	2080
Kcy_{simul} (Mpa)	1120	1380	1400	1300	1240	1200

LIST OF FIGURES AND FIGURES

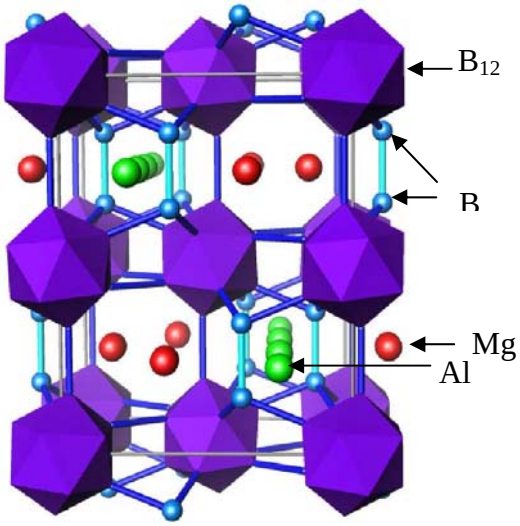

Fig. 10: Crystal Structure of the $AlMgB_{14}$

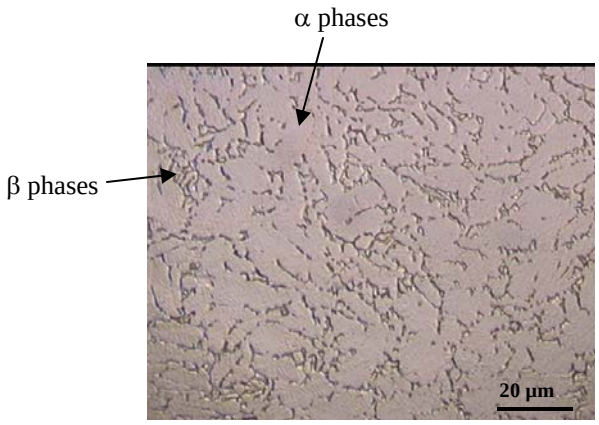

Fig. 2: Bulk titanium alloy microstructure

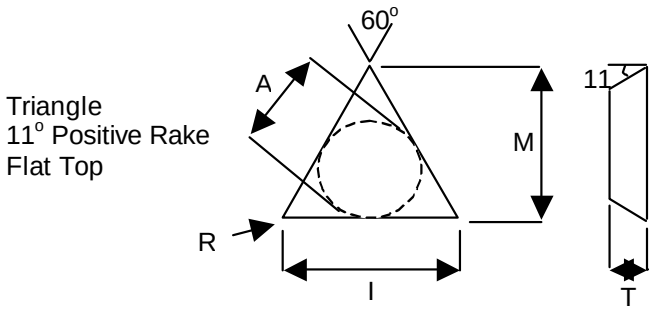

Fig. 3: Cutting tool geometry

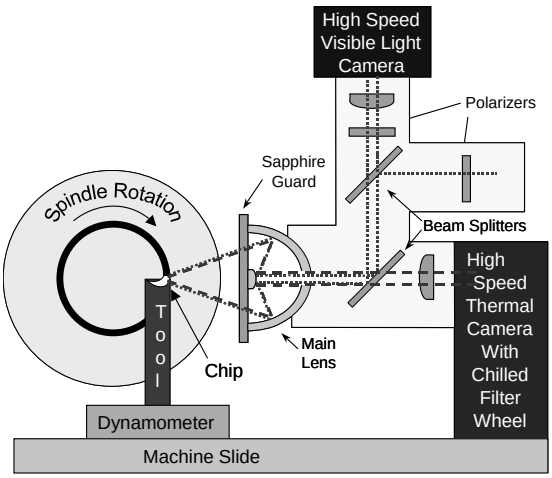

Fig. 4: Schema of the measurement setup

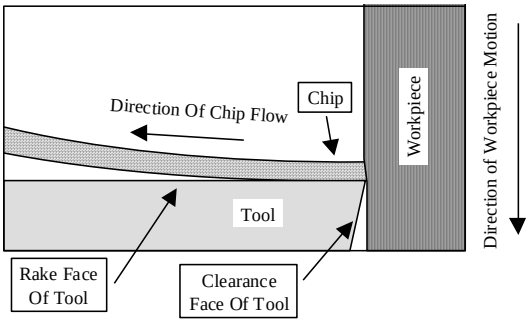

Fig. 5: Perspective of camera with an image example

a) Tool wear for WC-Co insert's material, test J-1

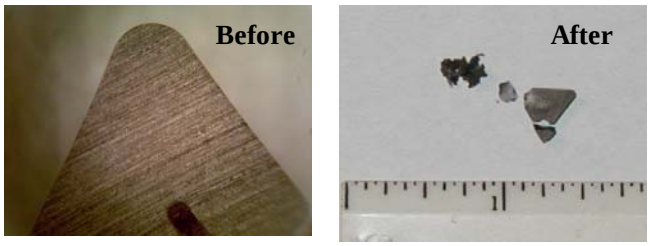

b) Tool wear for $AlMgB_{14}$ insert's material, test A-1

c) Tool wear for $AlMgB_{14}$ insert's material, test B-2

Fig. 6: Typical observed tool wear and failure

Fig. 7: The $AlMgB_{14}$ tool insert (on the right) produces a much more tightly curled chip (scale in inches)

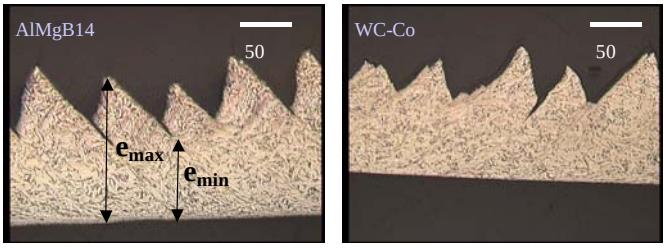

Fig. 8: Optical microscopy of a chip section obtained for both cutting tool materials

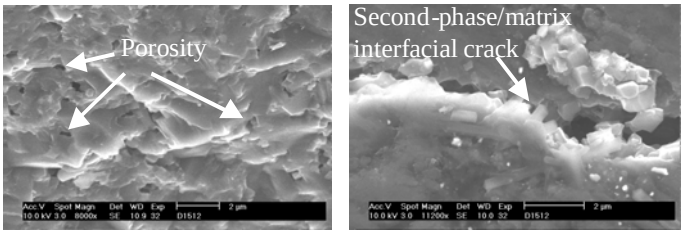

a) b)

Fig. 9: SEM of the fractured zone of $AlMgB_{14}$ tool material

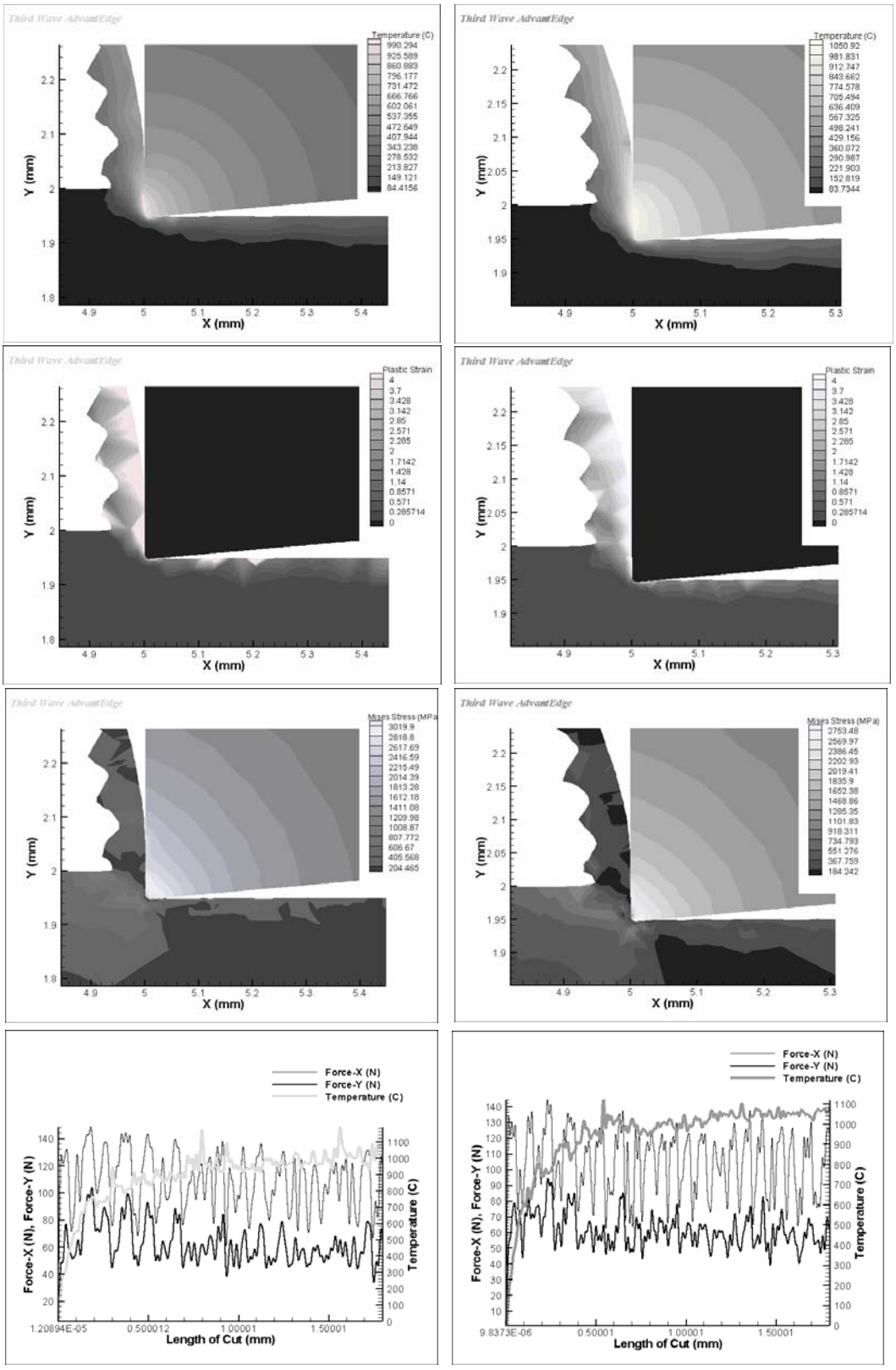

a) With Carbide-General tool material b) With Ceramic-General tool material

Fig. 10: Simulated results for Vc = 180 m/min